

Raman study of phonon modes and disorder effects in $\text{Pb}_{1-x}\text{Sr}_x\text{Se}$ alloys grown by molecular beam epitaxy

J. Chen and W. Z. Shen^{a)}

Laboratory of Condensed Matter Spectroscopy and Opto-Electronic Physics, Department of Physics, Shanghai Jiao Tong University, 1954 Hua Shan Road, Shanghai 200030, P. R. China

(Received 22 June 2005; accepted 18 November 2005; published online 10 January 2006)

We report phonon modes and alloy disorder effects of $\text{Pb}_{1-x}\text{Sr}_x\text{Se}$ alloys ($x \leq 0.3$) grown on BaF_2 (111) substrates by Raman spectroscopy measurements. On the basis of phonon modes in binary PbSe and SrSe, first-, second-, and high-order Raman scattering phonon frequencies of ternary $\text{Pb}_{1-x}\text{Sr}_x\text{Se}$ are observed, together with the deduction of the disorder activated modes due to the breakdown of the selection rule. The alloy disorder is found to play a more important role than the strain effect in $\text{Pb}_{1-x}\text{Sr}_x\text{Se}$, and has been further investigated by employing the special correlation model. The PbSe-like second-order features are also shown to broaden slightly and diminish in intensity with increasing Sr concentration, which has been attributed to a weak breakdown in the long-range order. © 2006 American Institute of Physics. [DOI: 10.1063/1.2159079]

I. INTRODUCTION

Considerable interest is being devoted recently to the lead salt IV-VI PbSe-based materials because of their unique optoelectronic and structural properties. Good quality PbSe-based thin films with excellent homogeneity can be epitaxially grown on low-cost BaF_2 (Refs. 1 and 2) and silicon³ substrates. Alloying Sr can widely tune the energy band gap (0.28–3.40 eV) within the ternary $\text{Pb}_{1-x}\text{Sr}_x\text{Se}$ system.¹ The absence of a heavy hole band in $\text{Pb}_{1-x}\text{Sr}_x\text{Se}$ thin films reduces the nonradiative Auger recombination rate by one or two orders of magnitude lower than that of narrow band gap III-V and II-VI materials.² This allows the appearance of stimulated emission at relatively low generation rates. Near room-temperature emission has been demonstrated in both PbSrSe/PbSe double heterostructure lasers⁴ and vertical-cavity surface-emitter lasers^{5,6} in the wavelength range from 3.0 to 5.0 μm . We have reported strong room-temperature infrared detection in $\text{Pb}_{1-x}\text{Sr}_x\text{Se}$ within 1.0–3.1 μm ,⁷ in addition to a detailed temperature-dependent absorption and photoluminescence investigation of $\text{Pb}_{1-x}\text{Sr}_x\text{Se}$ thin films and PbSrSe/PbSe quantum well structures for midinfrared laser applications.^{8,9} PbSr(Se,Te) with low dimensional structures are also found to be interesting candidate materials for thermoelectric applications.¹⁰

Despite the technological importance of the IV-VI alloy semiconductors, many microscopic vibrational properties of these systems are not well understood yet. In fact, knowledge of lattice vibrations in semiconductors will establish an important base in the fields of optoelectronics, heat transport, and quantum electronics. However, only a few studies of phonon modes for $\text{Pb}_{1-x}\text{Sr}_x\text{Se}$ alloy have been reported, including its two end members. Although Raman and reflection results have been published preliminarily by Yang *et al.*,¹¹ Kaneko *et al.*,¹² and Jiang *et al.*¹³ for the two binary PbSe and SrSe, respectively, the phonon information from their

analysis is still incomprehensive. In our previous work,¹⁴ we had employed the far-infrared reflection measurement to obtain the long-wavelength optical phonons and revealed mixed mode behavior in $\text{Pb}_{1-x}\text{Sr}_x\text{Se}$ using the modified random-element-isodisplacement model. However, the frequencies of the transverse-optical (TO) phonons of $\text{Pb}_{1-x}\text{Sr}_x\text{Se}$ were calculated through fitting and the longitudinal-optical (LO) phonons were estimated from the Kramers-Kronig calculation. More direct and accurate work upon phonon behavior in $\text{Pb}_{1-x}\text{Sr}_x\text{Se}$ is required. In addition to the phonon modes in $\text{Pb}_{1-x}\text{Sr}_x\text{Se}$ alloy, the potential fluctuations related to the alloy induced disorder on a microscopic scale are also one of the characteristic aspects of substitutional ternary semiconductors. In particular, alloy disorder in most of the mixed crystals plays a major role in the crystal quality issue, which needs more attention to be paid for.

Raman scattering not only is the most direct and nondestructive way to study the phonons of materials, but also can yield important information about structural order in the lattice on a scale of a few lattice constants. In this article, we investigate the Raman scattering of ternary $\text{Pb}_{1-x}\text{Sr}_x\text{Se}$ thin films for the complete phonon characteristics. The first-, second-, and high-order phonon scattering of $\text{Pb}_{1-x}\text{Sr}_x\text{Se}$ ($x \leq 0.3$) have been clearly assigned. In addition to the identification of the disorder activated modes caused by the breakdown of the selection rule, we have explicated the alloy induced disorder effects in ternary $\text{Pb}_{1-x}\text{Sr}_x\text{Se}$ alloys by the aid of the special correlation model (SCM).

II. EXPERIMENTAL DETAILS

Five $\text{Pb}_{1-x}\text{Sr}_x\text{Se}$ thin film samples were grown on freshly cleaved BaF_2 (111) substrates by molecular-beam epitaxy (MBE) techniques in an Intevac GEN II Modular system. PbSe, Se, and Sr were used as source materials. The Sr content x in the five samples is 0 (PbSe), 0.066, 0.171, 0.276, and 1.0 (SrSe), respectively, which have been confirmed by x-ray diffraction, absorption and photoluminescence

^{a)}Author to whom correspondence should be addressed; electronic mail: wzshen@sjtu.edu.cn

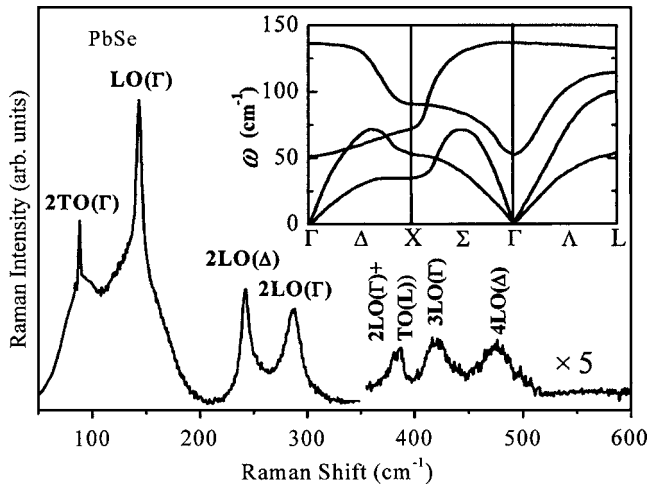


FIG. 1. The Raman spectrum of PbSe in the range from 50 to 600 cm^{-1} at room temperature. Shown in the inset is the calculated phonon dispersion curve of PbSe.

measurements.^{8,9} The thickness of the thin films is around 1 μm . Detailed growth conditions for the $\text{Pb}_{1-x}\text{Sr}_x\text{Se}$ thin films can be found elsewhere.^{2,8} The quite easy oxidation of Sr prevents us from growing good quality ternary PbSrSe thin films with high Sr content ($x > 0.3$) by MBE. Raman scattering measurements were carried out on a Jobin Yvon LabRAM HR 800 UV micro-Raman spectrometer at room temperature with a high resolution better than 0.5 cm^{-1} . By the aid of the confocal setup, this Raman system has a high signal distinguishing ability in the direction perpendicular to the thin film with a step scan resolution of 0.6 μm . The samples were excited using the 514.5 nm line from an Ar^+ laser at backscattering geometry. The incident laser was focused on the samples as a spot of 1 μm in diameter with the power less than 10 mW, and the acquisition time was 20 s.

III. RESULTS AND DISCUSSION

Figure 1 shows the Raman spectrum of the PbSe thin film ranging from 50 to 600 cm^{-1} taken in the $z(x, -)\bar{z}$ backscattering configuration. The observed dominant peaks are approximately 88 and 143 cm^{-1} . It is well known that PbSe possesses the rock-salt structure, and its first-order Raman scattering is symmetry forbidden due to the central inversion. However, calculation shows that both LO and TO phonons in PbSe on the (111)-oriented surface are not strictly Raman inactive in the backscattering geometry,¹¹ and slight violation of the translational symmetry may also activate such scattering. As a result, Raman scattering of forbidden LO modes in lead chalcogenides have been observed.^{15,16} To assign the Raman peaks to the phonon modes, we reference the theoretically calculated phonon dispersion curve (PDC) of PbSe (shown in the inset of Fig. 1) by considering the effects of van der Waals interactions, free-carrier doping, and three-body interactions in the framework of both-ions (anions and cations) polarizable rigid shell model.¹⁷ From the frequency point of view, it is straightforward that the observed Raman peaks around 143 cm^{-1} corresponds well to the first-order LO mode of PbSe. The TO phonon of $\sim 47 \text{ cm}^{-1}$ in the theoretical PDC is out of our experimental range due to the

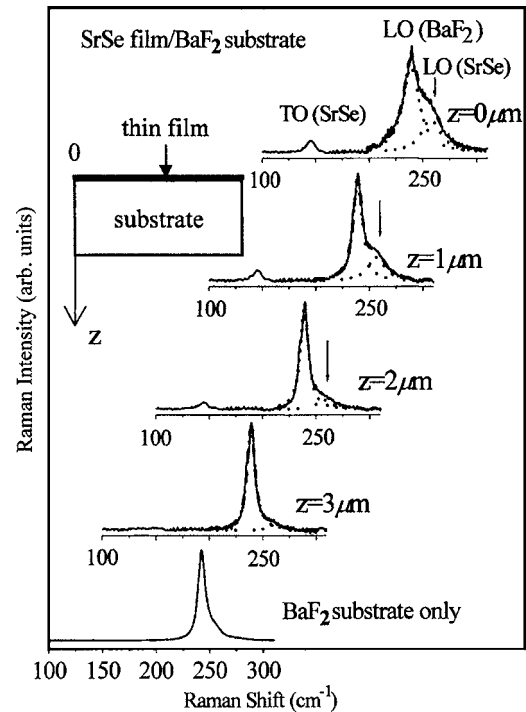


FIG. 2. Room-temperature Raman spectra of SrSe thin film with different laser focus depths, as well as the BaF_2 substrate, in the range of 100–300 cm^{-1} taken in a backscattering configuration. Solid curves: experimental data; dotted curves: two fitted Lorentz curves; and dashed curves: overall fitted results.

limitation of our Raman scattering system. Nevertheless, the second-order TO (2TO) phonon scattering at 88.4 cm^{-1} can be clearly observed in our spectrum, indicating that the TO mode phonon frequency is about 44.2 cm^{-1} for PbSe. This kind of frequency discrepancy is understandable, since the theoretical PDC is based on the bulk material, whereas our sample is thin film.

Besides the first-order phonon modes, the Raman spectrum in Fig. 1 also reveals the second- and high-order phonon scattering. According to the PDC, we can assign most of the Raman structures, and have marked the origin of all of the Raman peaks in Fig. 1, though the assignment for high-order modes may not be unique. In addition, we note that the feature at 243 cm^{-1} is very close to the LO frequency of the BaF_2 substrate, but we can easily rule out that possibility, since (i) the energy of incident photons (2.41 eV) is much higher than the band gap of PbSe (0.28 eV), and the light is absorbed entirely by the 1- μm -thick PbSe thin film, detection of the signal from the BaF_2 substrate is highly improbable; (ii) the intensity of this feature is observed to be weaker and weaker when the incident light is focused gradually from the PbSe film to the BaF_2 substrate (same as the schematic shown in the inset of Fig. 2); and (iii) this peak is found to redshift with the increase of Sr content in $\text{Pb}_{1-x}\text{Sr}_x\text{Se}$ alloys. We can therefore attribute it to the two-phonon scattering process $2\text{LO}(\Delta)$ from PbSe, which is in agreement with the value of 244 cm^{-1} in the PDC.

Figure 2 displays the Raman spectra of SrSe at different light focus depths along the layer from the thin film to the substrate. The peak at 145 cm^{-1} is from the TO phonon scattering of SrSe, which is close to the reported TO of 141 cm^{-1}

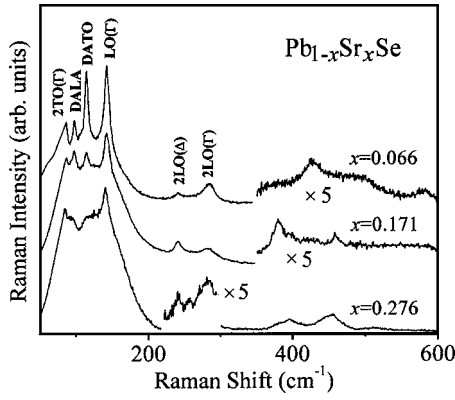


FIG. 3. The Raman spectra of $\text{Pb}_{1-x}\text{Sr}_x\text{Se}$ alloys ($x=0.066$, 0.171 , and 0.276) from 50 to 600 cm^{-1} .

by Kaneko *et al.*¹² and 142 cm^{-1} by Jiang *et al.*¹³ It should be noted that although the TO mode of SrSe has been observed by several experiments, no experimental data for the LO mode of SrSe are reported up to now. In our Raman spectra, the dominant feature is a broad structure at 242 cm^{-1} , together with a shoulder approximately 257 cm^{-1} , and no second- or high-order Raman scattering can be detected in SrSe. Compared with the Raman spectrum of the pure BaF_2 , the feature at 242 cm^{-1} is definitely from the LO phonon scattering of the BaF_2 substrate, because the energy of the incident photons is lower than the energy band gap of SrSe [3.40 eV (Refs. 13)], leading to the deep penetration of the incident laser into the substrate. However, the feature approximately 257 cm^{-1} is observed to be very sensitive to the focus depth, as shown in Fig. 2. When the focus spot is $3\text{ }\mu\text{m}$ beneath the film surface, only a sharp peak at 242 cm^{-1} is observed, and the Raman spectrum is almost the same as that from BaF_2 . While the focus depth gradually changes from $3\text{ }\mu\text{m}$ (BaF_2 substrate) to $0\text{ }\mu\text{m}$ (SrSe film surface), the feature approximately 257 cm^{-1} first appears and then becomes easier to be distinguished, accompanying the appearance of the SrSe TO phonons. These experimental results clearly demonstrate that the phonon scattering of 257 cm^{-1} originates from the SrSe thin film. Since the two structures centering at ~ 242 and 257 cm^{-1} are close to each other, we have used two Lorentz curves (dotted curves in Fig. 2) to separate them. The relative weak Raman intensity of SrSe LO phonons is due to the fact that the energy of the incident light is too low to excite the electrons from valence band to conduction band during the scattering process.

The clear understanding of the phonon modes in binary SrSe and PbSe establishes the base for proper analysis of the phonons and disorder effects in Sr incorporated $\text{Pb}_{1-x}\text{Sr}_x\text{Se}$ thin films. Figure 3 shows the Raman spectra of ternary $\text{Pb}_{1-x}\text{Sr}_x\text{Se}$ with the dominant PbSe-like LO mode at 143 cm^{-1} . The peaks at 87 , 241 , and 284 cm^{-1} in the spectra are the second-order PbSe-like modes, whereas the features in the range from 350 to 600 cm^{-1} are high-order scattering in $\text{Pb}_{1-x}\text{Sr}_x\text{Se}$ alloys. We have summarized all the observed first-, second-, and high-order phonon frequencies from Raman spectroscopy of the alloys in Table I, where the phonon information of PbSe and SrSe are also included. It is understandable that most of the phonon scattering in ternary $\text{Pb}_{1-x}\text{Sr}_x\text{Se}$ only has the PbSe-like characteristics due to the low concentration of Sr in ternary PbSrSe, where two-mode behavior has been observed for the studied concentration.¹⁴ Actually the observed SrSe-like LO mode in the high Sr content sample ($x=0.276$) and pure SrSe is very weak. Moreover, in comparison with the results in Ref. 14, we find that we have obtained higher frequencies for the SrSe-like LO modes in both $\text{Pb}_{0.724}\text{Sr}_{0.276}\text{Se}$ and pure SrSe by Raman scattering. We think that the discrepancy arises from the different experimental methodologies. In Ref. 14, we have first employed the far-infrared reflection spectra to yield the energies of TO phonons, and then estimated the LO phonon frequencies from the Kramers-Kronig calculation. Here, we use the straightforward Raman scattering to directly reveal the accurate results.

Besides the well assigned PbSe- and SrSe-like modes, we find two additional Raman features near 97 and 114 cm^{-1} in the alloys, which have comparable intensity to the dominant PbSe-like LO modes particularly in the $\text{Pb}_{0.934}\text{Sr}_{0.066}\text{Se}$ sample. Generally, we should attribute them to the SrSe-like phonon modes because $\text{Pb}_{1-x}\text{Sr}_x\text{Se}$ has two modes in that composition region.¹⁴ However, this kind of assignment is not suitable for these two Raman features (~ 97 and 114 cm^{-1}) because of the following arguments and experimental facts: (i) the intensity of these two features decreases with the increasing Sr concentration; (ii) their frequencies redshift as Sr increases, in contrast to the expected blueshift of the SrSe-like phonon modes; and (iii) in a Pb-rich sample of $\text{Pb}_{1-x}\text{Sr}_x\text{Se}$, a PbSe-like mode is expected to propagate, while a SrSe-like mode would be more like a gap mode with an amplitude of vibration decaying away from the impurity atom.

As we know, the alloying induced disorder will lead to

TABLE I. The first-, second-, and high-order Raman scattering phonon frequencies of the binary PbSe, SrSe, and the ternary $\text{Pb}_{1-x}\text{Sr}_x\text{Se}$ alloys ($x \leq 0.3$).

Samples	First-order Raman frequency (cm^{-1})						Second-order Raman frequency (cm^{-1})					High-order Raman frequency (cm^{-1})		
	PbSe-like			SrSe-like			PbSe-like		SrSe-like					
	TO(Γ)	Confined modes	LO(Γ)	TO	LO	2TO(Γ)	2LO(Δ)	2LO(Γ)	TO+LO	2LO				
PbSe	44.2	/	/	143.6	/	/	88.4	242.7	287.7	/	/	383 \pm 4	420 \pm 5	474 \pm 8
$\text{Pb}_{0.934}\text{Sr}_{0.066}\text{Se}$	43.6	98.2	115.1	142.8	/	/	87.3	241.1	284.7	/	/	365 \pm 3	426 \pm 4	582 \pm 10
$\text{Pb}_{0.829}\text{Sr}_{0.171}\text{Se}$	43.3	97.9	114.4	142.5	/	/	86.7	241.0	283.2	/	/	379 \pm 3	424 \pm 10	460 \pm 2
$\text{Pb}_{0.724}\text{Sr}_{0.276}\text{Se}$	42.3	96.3	113.5	140.6	/	255.3	84.5	240.6	280.9	396	513	455 \pm 1		
SrSe	/	/	/	/	145.0	257.0								

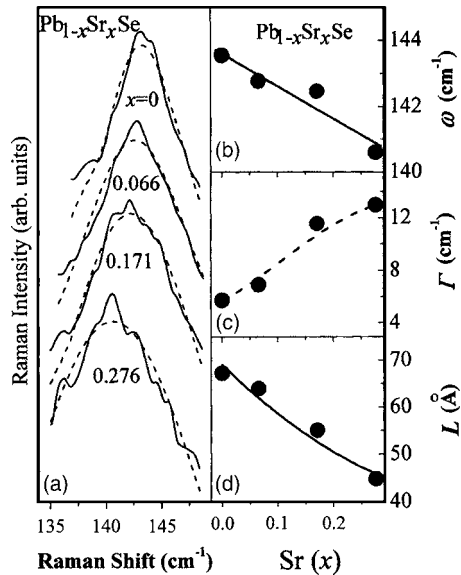


FIG. 4. (a) The PbSe-like LO phonon spectra of $\text{Pb}_{1-x}\text{Sr}_x\text{Se}$, where the redshift of the band is observed with increasing x . Dependence of (b) phonon frequency (c) linewidth, and (d) spatial correlation length of the PbSe-like LO phonons on Sr concentration in $\text{Pb}_{1-x}\text{Sr}_x\text{Se}$ alloys. The solid curves in (b) and (d) are the fitting results, whereas the dashed curve in (c) is guide to eyes.

the breakdown of the translational symmetry in mixed crystals and further bring new vibration modes. In this case, the phonons at Brillouin zone edges, where the phonon density of states are generally high, will also contribute to the first-order Raman scattering, which are usually referred as disorder activated (DA) modes. According to the PDC of PbSe, the frequencies of zone-edge longitudinal-acoustical (LA) and TO phonons are 99 and 113 cm^{-1} , respectively, which are quite close to those of the observed new modes. Therefore, we can attribute these two structures correspondingly to the DALA and DATO modes in the Pb-rich composition region. As such modes will only be activated by the presence of Sr atoms, we cannot detect these modes in the Raman scattering of pure PbSe, and the observation of these kinds of modes is taken as the evidence of disorder in the alloy.

Figure 4(a) plots the enlarged Raman feature of PbSe-like LO mode in $\text{Pb}_{1-x}\text{Sr}_x\text{Se}$. The frequency of the mode displays redshift with Sr concentration, and the full width at half maximum (FWHM) basically increases with x , as shown in Figs. 4(b) and 4(c). Further, Raman line shape of this mode displays a small asymmetric Lorentzian profile in $\text{Pb}_{1-x}\text{Sr}_x\text{Se}$ alloys, in contrast to the widely observed strong asymmetric Raman shape in some alloys such as $\text{CdS}_x\text{Se}_{1-x}$ ¹⁸ and $\text{In}_x\text{Ga}_{1-x}\text{As}$.¹⁹ This is because the strong asymmetry mainly arises from contribution of the DA mode at the low energy side, whereas the DA modes in our $\text{Pb}_{1-x}\text{Sr}_x\text{Se}$ are not overlapped by the LO mode.

It has been reported that the FWHM and the profile of Raman spectra will depend on both the strain from the lattice mismatch and alloy disorder of the thin film. In a mismatched heteroepitaxial system, the accommodation of the lattice mismatch will produce the strain if the epitaxial layer is thinner than a critical value t_c ; whereas for the thickness larger than t_c , the strain will be released. The lattice constant

of BaF_2 substrate is 6.202 Å, while the constant $d(\text{Pb}_{1-x}\text{Sr}_x\text{Se})$ of the thin film can be derived from the Vegard's law by linear interpolation between the value of $d(\text{PbSe})=6.124$ Å and $d(\text{SrSe})=6.225$ Å,²⁰ which yields $d(\text{Pb}_{1-x}\text{Sr}_x\text{Se})=6.124+0.101x$ (Å). According to the energy balance model,²¹ we can calculate the critical thickness t_c to be 0.1 μm for $\text{Pb}_{1-x}\text{Sr}_x\text{Se}$ layer on BaF_2 substrate, which is much thinner than the sample thickness of ~ 1 μm . As a result, the effect of strain on the Raman profile of PbSrSe is trivial. The weak strain effect in $\text{PbSrSe}/\text{BaF}_2$ material also exhibits itself in the frequency shift, which can be expressed on the dependency of Sr concentration by least square fitting as: $\omega_{\text{LO}}^{\text{PbSe-like}}(x)=143.4-9.89x$ [the solid line in Fig. 4(b)]. We find that the frequency shift in $\text{Pb}_{1-x}\text{Sr}_x\text{Se}$ is much smaller than that of the strain dominant alloys.²² In addition to the strain, the compositional fluctuation will also induce frequency shift of some Raman-active modes in alloys.²³

We now employ the well known SCM to analyze the disorder effects. The model is based upon the relaxation of the $q=0$ selection rule, induced by the microscopic nature of disorder in the alloys which yields a finite phonon mode correlation. The scattering intensity is described by the following formula²⁴:

$$I(\omega) \propto \int_0^1 \frac{\exp(-q^2L^2/4)d^3q}{[\omega - \omega(q)]^2 + (\Gamma/2)^2}, \quad (1)$$

where q is the wave vector in the unit of $2\pi/d$, d is the lattice constant of $\text{Pb}_{1-x}\text{Sr}_x\text{Se}$, L is the correlation length (Å), and Γ is the linewidth of the PbSe-like LO phonon. For the dispersion $\omega(q)$ of the LO phonon, results of the one dimensional linear-chain model can be used²⁵:

$$\omega(q)^2 = A + \{A^2 - B[1 - \cos(q\pi)]\}^{1/2}, \quad (2)$$

where the constants $A=(1/2)\omega_0^2(x)$ and $B=(1/2)\omega_0^4(x)m\mu/(m+\mu)^2$ with the Se mass of $m_{\text{Se}}=78.96$ amu and weighted mean mass of $\mu=(1-x)M_{\text{Pb}}+xM_{\text{Sr}}$ ($M_{\text{Pb}}=207.2$ amu and $M_{\text{Sr}}=87.62$ amu). $\omega_0(x)$ is the phonon frequency at the zone center. The spatial correlation length L can be assumed as a measure of the extent to which the lattice is ordered, since the disruption in the periodicity is the cause of the finite spatial correlation of the phonon wave function. For simplicity, the integration on the right-hand side of Eq. (1) is taken in a spherical Brillouin zone.

Figure 4(a) plots the least square fit (dashed curves) of Eq. (1) to the experimental data (solid curves) of the PbSe-like LO phonons in $\text{Pb}_{1-x}\text{Sr}_x\text{Se}$. Figures 4(c) and 4(d) show the fitted parameters Γ and L as a function of Sr concentration. With increasing Sr content, Γ increases whereas L decreases. The larger Γ value implies the shorter phonon relaxation time leading from the higher density of defects or dislocations, which are induced mainly by the alloy disorder in $\text{Pb}_{1-x}\text{Sr}_x\text{Se}$. As the PbSe-like phonon modes are considered to be localized in the PbSe regions, L represents the average size of the localized region of PbSe-like phonons. The calculated phonon coherence length L decreases with increasing Sr concentration, which indicates that the phonon extended region becomes smaller in higher Sr content as a result of the alloy disorder. The large disorder in $\text{Pb}_{1-x}\text{Sr}_x\text{Se}$

reflected in Raman scattering process is mainly due to the fact that the substitutional element Sr is from a different group (II for Sr versus IV for Pb) with different outer electrons. Furthermore, we also find that the degree of disorder is approximately proportional to the product of Sr and Pb compositions $x(1-x)$ and the solid curve in Fig. 4(d) is the fitted result of $L=69-116x(1-x)$ (Å), revealing the maximum disorder when the Sr atoms substitute half of the Pb atoms in PbSe.

The second-order Raman scattering in ternary $\text{Pb}_{0.934}\text{Sr}_{0.066}\text{Se}$ and $\text{Pb}_{0.829}\text{Sr}_{0.171}\text{Se}$ is believed to be PbSe-like according to the phonon frequencies (see Table I). Although in Raman scattering of a relatively high Sr incorporated $\text{Pb}_{0.724}\text{Sr}_{0.276}\text{Se}$ sample, in addition to the PbSe-like phonons, we can identify the second-order SrSe-like phonons at $396\text{ cm}^{-1}(\text{TO}+\text{LO})$ and 513 cm^{-1} (2LO), together with the first-order SrSe-like LO phonons as mentioned previously. Not only the PbSe-like first-order modes, but also the observed PbSe-like second-order phonons exhibit redshift with increasing Sr content. Figures 1 and 3 have clearly displayed the rapid degradation of the fairly sharp PbSe-like $2\text{TO}(\Gamma)$, $2\text{LO}(\Delta)$, and $2\text{LO}(\Gamma)$ second-order features. For pure PbSe, these Raman structures are narrow and well observed above the underlying two-phonon continuum. However, in ternary $\text{Pb}_{1-x}\text{Sr}_x\text{Se}$, these features decrease in relative strength and broaden slightly. Since second-order Raman process is a sensitive test of crystalline quality, we interpret these results as the evidence of weakly diminishing long-range order with increasing Sr concentration, which is in good agreement with our previous discussion.

IV. CONCLUSIONS

In summary, we have reported the characteristics of the first-, second-, and high-order scattering in $\text{Pb}_{1-x}\text{Sr}_x\text{Se}$ (for $x \leq 0.3$) and PbSe, as well as the TO and LO phonons in SrSe by Raman scattering measurements. The disorder induced DATO and DALA modes in ternary $\text{Pb}_{1-x}\text{Sr}_x\text{Se}$ have been observed. The alloying disorder plays a key role in $\text{Pb}_{1-x}\text{Sr}_x\text{Se}$ alloy in the Raman scattering process and the calculated phonon coherence length L in SCM demonstrates

that the disorder increases with Sr concentration, which also can be confirmed by the second-order PbSe-like structures in $\text{Pb}_{1-x}\text{Sr}_x\text{Se}$.

ACKNOWLEDGMENTS

This work was supported in part by the Natural Science Foundation of China under Contract Nos. 10 125 416 and 60 576 067, as well as TRAPOYT of the National Minister of Education. The authors would like to acknowledge Dr. H. Z. Wu at Zhejiang University for providing the samples.

- ¹A. Lambrecht, N. Herres, B. Spanger, K. Kuhn, H. Böttner, M. Tacke, and J. Evers, *J. Cryst. Growth* **108**, 301 (1991).
- ²P. J. McCann, K. Namjou, and X. M. Fang, *Appl. Phys. Lett.* **75**, 3608 (1999).
- ³P. Müller, H. Zogg, A. Fach, J. John, C. Paglino, A. N. Tiwari, M. Krejci, and G. Kostorz, *Phys. Rev. Lett.* **78**, 3007 (1997).
- ⁴U. P. Schiessl and J. Rohr, *Infrared Phys. Technol.* **40**, 325 (1999).
- ⁵C. L. Felix, W. W. Bewley, I. Vurgaftman, J. R. Lindle, J. R. Meyer, H. Z. Wu, G. Xu, S. Khosravani, and Z. Shi, *Appl. Phys. Lett.* **78**, 3770 (2001).
- ⁶F. Zhao, H. Wu, A. Majumdar, and Z. Shi, *Appl. Phys. Lett.* **83**, 5133 (2003).
- ⁷H. F. Yang, W. Z. Shen, and Q. J. Pang, *Appl. Phys. Lett.* **81**, 2394 (2002).
- ⁸W. Z. Shen, H. F. Yang, L. F. Jiang, K. Wang, G. Yu, H. Z. Wu, and P. J. McCann, *J. Appl. Phys.* **91**, 192 (2002).
- ⁹W. Z. Shen, *Appl. Phys. A* **80**, 389 (2005).
- ¹⁰H. Beyer, J. Nurnus, H. Büttner, A. Lambrecht, L. Schmitt, and F. Vülklein, *Mater. Res. Soc. Symp. Proc.* **225.1-6**, 626 (2001).
- ¹¹A. L. Yang, H. Z. Wu, Z. F. Li, D. J. Qiu, Y. Chang, J. F. Li, P. J. McCann, and X. M. Fang, *Chin. Phys. Lett.* **17**, 606 (2000).
- ¹²Y. Kaneko, K. Morimoto, and T. Koda, *J. Phys. Soc. Jpn.* **51**, 2247 (1982).
- ¹³L. F. Jiang, W. Z. Shen, and H. Z. Wu, *J. Appl. Phys.* **91**, 9015 (2002).
- ¹⁴J. Chen and W. Z. Shen, *J. Appl. Phys.* **93**, 9053 (2003).
- ¹⁵S. V. Ovsyannikov, Y. S. Ponosov, V. V. Shchennikov, and V. E. Mogilenskikh, *Phys. Status Solidi C* **1**, 3110 (2004).
- ¹⁶G. D. Smith, S. Firth, R. J. H. Clark, and M. Cardona, *J. Appl. Phys.* **92**, 4375 (2002).
- ¹⁷K. S. Upadhyaya, M. Yadav, and G. K. Upadhyaya, *Phys. Status Solidi B* **229**, 1129 (2002).
- ¹⁸J. L. Shen, I. M. Chang, Y. M. Chu, and Y. F. Chen, *Phys. Rev. B* **50**, 1678 (1994).
- ¹⁹K. Wiesauer and G. Springholz, *Phys. Rev. B* **69**, 245 313 (2004).
- ²⁰G. Yu, L. F. Jiang, W. Z. Shen, and H. Z. Wu, *J. Phys. D* **35**, 157 (2002).
- ²¹R. People and J. C. Bean, *Appl. Phys. Lett.* **47**, 322 (1985).
- ²²T. Prokofyeva, T. Sauncy, M. Seon, M. Holtz, Y. Qiu, S. Nikishin, and H. Temkin, *Appl. Phys. Lett.* **73**, 1409 (1998).
- ²³C. H. Perry, F. Lu, and F. Navamar, *Solid State Commun.* **88**, 613 (1993).
- ²⁴C. Parayanthal and F. H. Pollak, *Phys. Rev. Lett.* **52**, 1822 (1984).
- ²⁵C. F. Klingshirm, *Semiconductors Optics* (Springer, New York, 1995).